THE JOURNAL OF PHYSICAL CHEMISTRY B

Article

pubs.acs.org/JPCB

Single-Molecule Force Spectroscopic Studies on Intra- and Intermolecular Interactions of G-Quadruplex Aptamer with Target Shp2 Protein

Xue-Qin Zhao, Jie Wu, Jing-Hong Liang, Jia-Wei Yan, Zhi Zhu, Chaoyong James Yang,* and Bing-Wei Mao*

State Key Laboratory of Physical Chemistry of the Solid Surfaces, Department of Chemistry, Department of Chemical Biology, College of Chemistry and Chemical Engineering, Xiamen University, Xiamen 361005, PR China

Supporting Information

ABSTRACT: With widespread applications in biosensors, diagnostics, and therapeutics, much investigation has been made in the structure of the G-quadruplexes and mechanism of their interactions with protein targets. However, in view of AFM based single-molecule force spectroscopic (SMFS) studies of G-quadruplex systems, only bimolecular approaches have been employed. In this article, we present an improved dual-labeling approach for surface immobilization of G-quadruplex DNA apatmers for investigation of intramolecular interaction from an integral unimolecular G-quadruplex system. The melting force of HJ24 G-quadruplex aptamer in the presence of K^+ has been successfully measured. It has been found that dynamic equilibrium exists between unfolding and folding structures of the HJ24 aptamer even in pure water. We also investigated the interactions between the HJ24 aptamer and its target protein (Shp2) under the same solution condition. The HJ24/Shp2 unbinding force in the absence of K^+, 42.0 pN, is about 50% smaller than that in the presence of K^+, 61.7 pN. The great reduction in force in the absence of K^+ suggests that the stability of G-quadruplex secondary structure is important for a stable HJ24/Shp2 binding. The methodology developed and demonstrated in this work is applicable for studying the stability of secondary structures of other unimolecular G-quadruplex aptamers and their interactions with target proteins.

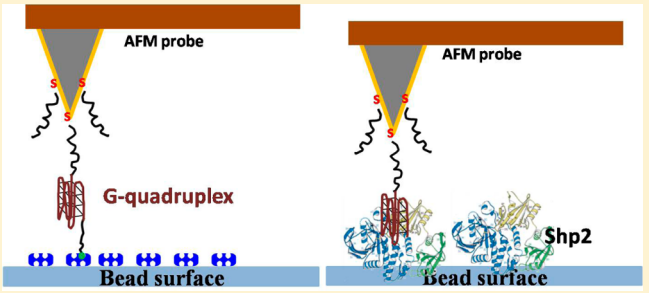

INTRODUCTION

Guanine (G)-rich oligonucleotides can self-assemble into G-quadruplex structures via hydrogen bonding and stacking of the G-quartet structures upon one another and the coordination of charges by monovalent cations in the central cavity of the G-quadruplexes.[1−5] One most extensively characterized example of G-quadruplex DNA is found in telomeres at the ends of eukaryotic chromosomes, which has played an important role in gene regulation[6,7] and served as the target of drugs for cancer treatment.[8] As such, the G-quadruplexes created in vitro tend to form blocks for nanostructures[9,10] and nanomachines.[11] Their high affinity and selectivity with target proteins make them ideal and powerful tools in biosensors[12,13] and potent pharmaceuticals.[14] Understanding of the conformational stability of G-quadruplexes and the influence by the binding of other molecules is of crucial importance.

Traditional molecular recognition methods such as fluorescence spectroscopy, UV−vis spectroscopy, surface plasmon resonance (SPR), nuclear magnetic resonance (NMR), and X-ray diffraction techniques (XRD) have been employed to study the binding mechanism and properties of aptamer/protein complexes.[15−18] However, information obtained by these approaches is averaged responses of molecular ensembles of systems. Single molecule techniques deal with molecules one at a time; therefore, information obtained is from individual molecules in a heterogeneous sample in the absence of undesirable interference of other molecules. Statistical analysis of data is performed to reveal the fluctuating behaviors of single molecule events,[19,20] which is a reflection of the intrinsic properties of the system at single molecule level which is otherwise hidden in the measurements by traditional techniques. Single molecular fluorescence resonance energy transfer (FRET) has been used to investigate the structure of G-quadruplexes with and without bound ligands.[21] However, the incorporation of relatively large fluorophores may perturb the structure under investigation. Single molecule force spectroscopic (SMFS) based on atomic force microscopy (AFM) has found wide applications in biology due to its piconewton force sensitivity, nanometer positional accuracy, and ability to study molecular interactions down to single molecule resolution.[22−24] It serves as a promising and complementary tool to traditional ones as well as single

Received: April 12, 2012
Revised: August 21, 2012
Published: August 28, 2012

dx.doi.org/10.1021/jp303518b | J. Phys. Chem. B 2012, 116, 11397−11404

molecule techniques for studying molecular interactions. Hereby, the forces acting between a sharp tip and a flat surface may be probed by measuring the deflection of the cantilever, onto which the tip is attached. Specific interaction forces can be investigated by functionalizing the tip and the surface, respectively. For example, the rupture forces of intermolecular binding such as receptor−ligand,[25] antigen−antibody,[26] and pathogen−host[27] have been monitored, and the unfolding events of the protein such as the elegant giant protein kinase structure[28] and separation of genetic RNA with its protein coat[29] have been examined by monitoring the force variation. Especially, the forces corresponding to sequential "unzipping" of double-stranded DNA have reached the resolution that can identify mismatch of a single DNA base pair.[30,31]

The binding affinities between G-quadruplex aptamers and target proteins have also been studied by SMFS.[32−34] For this purpose, the melting forces of the G-quadruplex structure need to be measured and understood first. However, there is a noticeable lack of investigations in this aspect. G-quadruplexes can be formed from uni-, bi-, and tetramolecular guanine-rich DNA strands. In 2009, the Kumar Sinniah group initially reported a SMFS study of a bimolecular G-quadruplex system,[35] in which the two single strand parts were fixed on the tip and substrate, respectively. This was followed by the work of unimolecular G-quadruplex study by Nguyen et al in 2011, but the unimolecular G-quadruplex was separated into two parts for immobilizing onto the tip and surface, respectively,[36] so that the corresponding "bipartite" concept was put forward in that work. However, the melting forces thus measured might not reflect the true intramolecular interactions of the molecular G-quadruplex as the original G-quadruplex structure may not be reached through recombination of the two single strand parts fixed at the tip and surface. In addition, the results obtained are usually difficult to be used for further quantitative comparisons with those of G-quadruplex aptamer−protein interactions because small differences in experimental conditions such as different type of probes or different solution conditions may drastically affect the measurements.[37] This might explain the lack of literature in the correlation of G-quadruplex structural stability and the binding affinity to target protein.

In this work, we report an improved dual-labeling approach of G-quadruplex aptamer for surface attachment, which allows one to undertake investigations of the structural stability of G-quadruplex aptamers and their interactions with target proteins. A G-quadruplex aptamer, HJ24, which is a unimolecular G-quadruplex structure,[38] against oncogenic protein Shp2 is chosen as a model in this work. Protein Shp2 is a member of the protein tyrosine phosphatases (PTPs), which regulates numerous signaling events that are virtually fundamental to all essential cellular processes. It is well established that dysfunction of Shp2 is associated with cancers, metabolic syndromes, and autoimmune disorders. The active aptamer conformation that binds to Shp2 consists of a intramolecular G-quadruplex structure.[38] Figure 1 outlines the strategy of the approach, wherein the G-quadruplex DNA is thiolated at its 3′ end for covalently anchoring to a gold tip and biotinylated at the 5′ end for binding with the streptavidin (SA) modified at the substrate surface. Since the binding of biotin with SA is sufficiently strong, once such binding occurs, the G-quadruplex molecule will be extended upon continuous retracting of the probe, leading to characteristic force curves. The rupture forces of the thiolated 3′ and biotinylated 5′ ends may also appear on the force curve depending on their relative strength and the probe reacting length. These measurements for both structural stability of G-quadruplex aptamers and their interactions with target proteins are fulfilled under the same solution and by using the same type of probes. Investigations of the sequence of force transitions originating from intra- and intermolecular interactions help reach a correct understanding of the aptamer−target protein interaction.

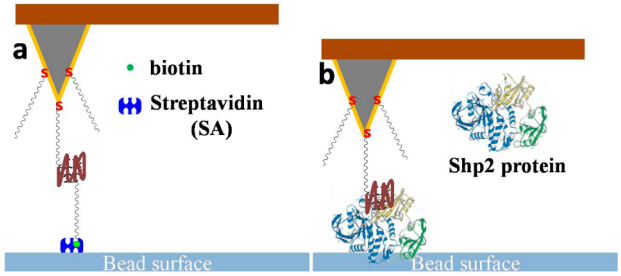

Figure 1. Schematic illustration of AFM-based single molecule force spectroscopic study for the intramolecular interaction G-quadruplex DNA (a) and intermolecular interaction with oncogenic Shp2 protein (b). The G-quadruplex DNA having four G-rich domains (colored in brown) is dual-labeled (5′-biotin, 3′-thiol) through two linker DNA molecules (T_{20} sequence, black). Gold-coated AFM probes are modified with a SAM of the dual-labeled G-quadruplex DNA through the thiolated 3′ end in dilution by thiolated spacer-DNA (also T_{20} sequence) at 1:5 molar ratio.

EXPERIMENTS

Materials and Instrumentation. All sequences of oligonucleotides were synthesized in house on a Polygen 12-Column DNA/RNA synthesizer and purified by an Agilent 1100 series HPLC system (Agilent Technologies, Inc.) on a reverse-phase C18 column. All other chemicals used in this work were purchased from Sigma. Ultrapure water from a Millipore Milli-Q system (>18 MΩ·cm) was used to prepare solutions.

AFM imaging and SMFS measurements were performed on an Agilent 5500ILM SPM (Agilent Technologies, Inc.) equipped with a N9520A scanner with a scan size of 10 μm in x−y and 2.08 μm in z directions. Gold coated silicon probes (NT-MDT) with a nominal force constant of 0.01−0.08 N/m (CSG/11 Au) and 5.5−22.5 N/m (NSG/10) were used for force measurements and imaging, respectively. All experiments were carried out in a homemade liquid cell containing either ultrapure water or K^+ containing solutions.

Commercially available agarose beads (average particle size 34 μm, GE Healthcare) were used as the receptor substrate onto which either SA or Shp2 protein was attached. For control experiments, the beads were modified with bovine serum albumin (BSA) only.

AFM Tip Functionalization. As a model G-quadruplex aptamer HJ24, the G-rich DNA,[38] whose sequence is shown in Table 1, was dual-labeled by a thiolated linker DNA at the 3′ end (3′-T_{20}-SH) and/or biotin at the 5′ end (5′-T_{20}-bio). The aptamer was heated to 95 °C for 5 min followed by incubation for 15 min in ice. After staying for 1 h at RT, the G-rich DNA molecule was stored at 4 °C. For AFM tip functionalization, the labeled G-rich DNA molecules of 1 μM were 1:5 diluted by the thiolated spacer DNA (SH-T_{20}). Au-coated AFM probes (CSG11/Au) were treated with acetone and isopropanol for 30 min, respectively, and then washed with ultrapure water.

dx.doi.org/10.1021/jp303518b | J. Phys. Chem. B 2012, 116, 11397−11404

Table 1. DNA Sequences (3′ → 5′) Employed in This Study

oligo	sequence
dual-labeled HJ24 G-quadruplex DNA (SH-HJ24-bio)	5′-bio-T_{20}-AGGGGGTTTTGGTGGGGGGGGCTGGGTTGTCTTGGGGGTGGGCT-T_{20}-SH-3′
dual-labeled random sequence DNA (control DNA)	5′-bio-T_{20}-CACCCCCTTTTGGTCCCCCCCCCCTGGGTTGTCTTCCCCCTCCCCT-T_{20}-H-3′
thiol-labeled HJ24 G-quadruplex DNA (SH-HJ24)	CAGGGGGTTTTGGTGGGGGGGGCTGGGTTGTCTTGGGGGTGGGCT-T_{20}-SH-3′
thiol-labeled random sequence DNA (random DNA)	CACCCCCTTTTGGTCCCCCCCCCCTGGGTTGTCTTCCCCCTCCCCT-T_{20}-SH-3′
spacer DNA (SH-T_{20})	T_{20}-SH-3′
T_{20}	T-T-T-T-T-T-T-T-T-T-T-T-T-T-T-T-T-T-T-T

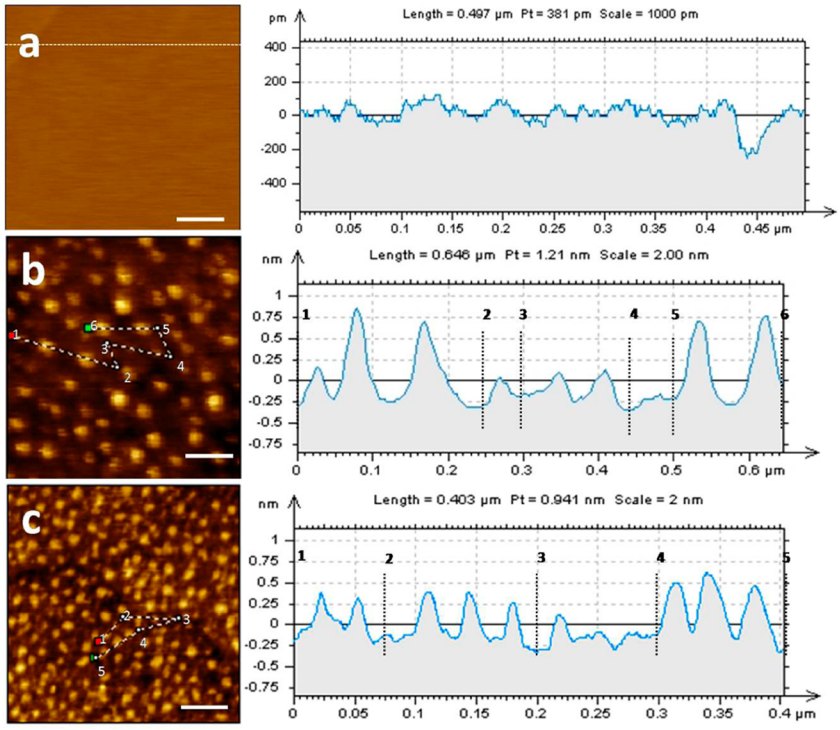

Figure 2. AFM images and sectional analysis. (a) Bare Au(111) surface, (b) SAM of dual-labeled G-quadruplex DNA (SH-HJ24-bio) on Au(111) surface with dilution of the DNA spacer T_{20}-SH (1:5), (c) SAM of thiol-labled G-quadruplex DNA (SH-HJ24) on Au(111) surface with dilution by the DNA spacer T_{20}-SH (1:5). All images were recorded under acoustic AC mode in a 60 mM K^+ containing solution. Lateral scale bars: 100 nm.

Subsequently, the probes were incubated in 100 μL aptamer containing solution at 4 °C for 20 h in order to immobilize the G-rich DNA molecules onto the AFM tip. This was followed by washing with ultrapure water to remove the unattached aptamers. The spring constants of the modified AFM cantilevers were calibrated using the thermal noise method, which ranges from 55 to 67 pN/nm.

Force Spectroscopic Measurements and Data Analysis. In each experiment, several hundreds of force curves were collected by repeatedly approaching the AFM tip in contact with the surface at a fixed force of 150 pN, holding in place for some time to allow binding to occur, and then retracting from the surface at a loading rate of 0.05 μm/s. Each curve was recorded at a different position on the surface more than five beads away from the previous measurement. Each experiment was repeated twice at least.

Histograms were built for rupture forces of interest from selected force curves that exhibit clear force transitions. The selection rate is usually ca. 10−60% of the total original force curves. The most probable rupture forces were determined by Gaussian fitting of the force histograms. For determining the stability of the secondary structure of the G-quadruplex DNA molecule, only those rupture forces that appear just preceding the last rupture force of biotin−SA (124.4 pN) and within 16.3 nm in retracting distance from the location that biotin−SA is ruptured were selected for building the histograms. The distance range defined for meaningful stretching of G-quadruplex DNA is an estimated total extending length of the 45 bases contained in one HJ24 molecule (0.43 nm/base[39] for ssDNA) after subtracting the length of the G-quadruplex structure, assuming an axial extending of 3.09 nm per three layers of the G-quadruplex structure.[40] Rupture forces bigger than 124.4 pN most likely resulted from the rupture events of several molecules.

AFM Imaging. Au(111) surfaces, which were used to study the immobilization of HJ24 G-quadruplexes on gold surface, were (111) facets of single-crystal beads. Prior to each experiment, the working surface was subjected to electrochemical polishing and flame annealing in H_2 followed by cooling under N_2 atmosphere.[41] The HJ24 G-quadruplex molecules were immobilized onto Au(111) surfaces using the same procedure as for AFM tip functionalization mentioned above. AFM images of the Au(111) surface were taken in liquid under acoustic AC mode with scan rates of 0.5−1.0 lines/s. When necessary, the AFM images were processed by flattening

dx.doi.org/10.1021/jp303518b | J. Phys. Chem. B 2012, 116, 11397−11404

with Pico image Basic software in order to remove the background slope.

RESULTS AND DISCUSSION

AFM Characterization of HJ24 Aptamer Functionalized on Au. For a molecule to interact with a target molecule, the molecules should retain sufficiently high mobility so that they can find each other with high probability.[23] In this work, the G-rich DNA HJ24 was attached onto the AFM tip via a flexible DNA molecular linker of T_{20} sequence, which confers higher probability for the G-rich DNA to bind with the attached proteins at the surface. A thiolated spacer DNA SH-T_{20} was used as the spacer. Here the advantages of using a mixed monolayer are worth emphasizing: The employment of the spacer molecules prevents flat falling of the G-rich DNA and reduces the undesirable coupling among the molecules under investigation, which are necessary for single molecule detection. Moreover, the G-rich DNA folds quite effectively in the binding solution into the respective intrastand G-quadruplex structure, which can then specifically bind to the Shp2 protein. The 1:5 dilution of the G-rich DNA greatly reduces the possibility to form interstand G-quadruplexes during folding.[42]

To investigate the monodispersity of the diluted labeled G-rich DNA, we applied AFM measurements to the Au(111) surface functionalized with the G-rich DNA. The employment of smooth single crystalline Au(111) surfaces enables the G-rich DNA to be distinguished from the background spacer DNA(SH-T_{20}). The image in Figure 2a reveals that the bare Au(111) surface without the DNA treatment has a peak-to-valley roughness of 0.2 nm, equivalent to a monatomic step height of the Au surface. Figure 2b and c show the images of the diluted dual-labeled and thiol-labeled G-rich DNA molecular layer at Au(111), respectively. Bright spots of different sizes were observed for both the dual-labeled and thiol-labeled G-rich DNA molecular layer. In Figure 2b, the globular bright spots are of two sizes. The smaller ones are 0.2−0.3 nm in height and ca. 30 nm in diameter, and the larger ones are around 1 nm in height and 60 nm in diameter. In Figure 2c, the larger ones are around 0.8 nm in height and 40 nm in diameter, and the smaller ones are almost identical to the those smaller ones in Figure 2b. The surface coverage of the larger and smaller spots is roughly 1:5, in agreement with the 1:5 dilution of the G-rich DNA and the spacer DNA molecules. These results suggest that the smaller spots correspond to the spacer DNA molecules and the larger spots the G-rich DNA molecules. Literature work has shown that an unlabeled G-rich DNA appears in a spot with a size of about 41.7 nm in the AFM image, which is bigger than its actual size[43] because of the tip shape convolution effect. Considering that the diameter of the tip employed in this work is typically of a curvature radius of about 50 nm which was confirmed by SEM inspection, the bright spots of 40−60 nm in diameter in Figure 2b and c are recognized to be likely within the size regime of a single G-rich DNA molecule. In addition, the thiol-labeled G-rich DNA (SH-HJ24) appears with a size at the smaller side of the 40−60 nm size regime, which is reasonable because the absence of the bio-T_{20} label remarkably reduces the size of the G-rich DNA molecule. It may be concluded therefore the labeled G-rich DNA molecules are monodispersed among the spacer DNA molecules and the neighboring G-rich DNA molecules are sufficiently apart, which provides the basis for single molecule force measurements.

Secondary Structure Stability of HJ24 G-Quadruplex Aptamer. *Force Curve Selection and Analysis.* As has been shown in Figure 1a, the stability of the secondary structure of the HJ24 G-quadruplex aptamer may be investigated by measuring its melting force before the rupture of the biotin−streptavidin bond. Typical force curves of the dual-labeled HJ24 G-quadruplex DNA (SH-HJ24-bio) are presented in Figure 3.

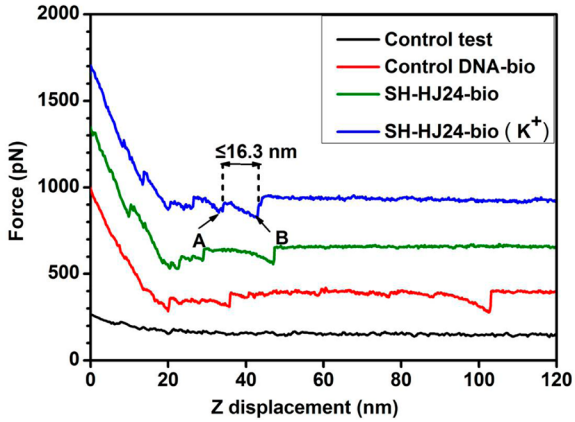

Figure 3. Typical force curves of dual-labeled G-quadruplex in solution with 60 mM K^+ (blue curve), without K^+ (green curve), dual-labeled random sequence DNA (red curve), and control test (black curve). The force transition indicated by arrows A and B correspond to melting force and bio−SA rupture force, respectively. All curves were recorded upon tip retracting.

Generally, large variation was observed in force curves, which can be traced back to the stochastic nature of the unfolding process in the single molecule limit.[44] To extract reliable and quantitative information, a statistical analysis of a large number of force curves should be performed. In this respect, proper selection of the potentially interesting force curves from thousands of raw force curves is crucial, which should be carefully performed with appropriate and reliable criteria.[45]

For SMFS study of the intramolecular interaction of G-quadruplex DNA molecule in this work, which involves experimental procedures of tip in contact with and then withdrawn from the SA on the surface of a bead, various complex rupture processes must be carefully anatomized. Specifically, intramolecular binding forces and thus the stability of the secondary structure of the G-quadruplex should be distinguished from those of the Au−S and bio−SA binding forces at the two labeling ends of the G-quadruplex molecule. Here, as a general consensus, the thiolated end of the dual-labeled G-quadruplex molecule coupled to the gold-coated AFM tip via a strong Au−S bond (typically 1.4 nN[46]) is regarded to be of strong covalent nature, whereas the intermolecular bio−SA bond at the biotinylated end is considered as the strongest noncovalent biological interaction known. The covalent bond of 1−2 nN is at least 10 times stronger than the receptor−ligand bond such as the strong bio−SA bond.[23] On the other hand, the melting force of G-quadruplex molecules documented in the literature ranges from 23 to 60 pN[47] and should be sufficiently smaller than that of the bio−SA bond. This gives a force sequence of melting of HJ24 < bio−SA bond < Au−S bond. Hence, we expect that in the presence of K^+, as the AFM probe retracts, the G-quadruplex secondary structure extends first. This is followed by breaking of the bio−SA complex, which ends the meaningful

force measurement. Representative force curves are shown in Figure 3. Since the aptamer HJ24 used in this study is an intramolecular single-stranded G-quadruplex structure, only one significant rupture peak can be observed from melting of the secondary structure in the force−extension measurements because of the restriction in force sensitivity of AFM. The last force transition preceding the rupture of the bio−SA bond should correspond to the melting force of the G-quadruplex secondary structure, provided that the total tip traveling distance is within 16.3 nm from the last detected bio−SA rupture. Force transition within 16.3 nm from the last one only appears in the G-quadruplex containing system in the presence of K^+. For the control experiment of random sequence DNA with K^+, no clear force transitions are observed. The spikes other than the mentioned force transitions are attributed to noises arising from the nonspecifically adsorbed species.

Rupture Force of Bio−SA. Three additional control experiments were carried out to confirm that the last measured forces were from that of biotin/SA interaction. (1) A bare SMFS tip without the attached G-quadruplex DNA HJ24 was used to interrogate the surface-immobilized SA (bare tip/SA bead). (2) A tip attached with dual-labeled HJ24 G-quadruplex DNA was used to interrogate a surface without SA protein (HJ24-bio tip/BSA bead). (3) The SA-coated beads were incubated overnight in a biotin solution so that all free binding sites of the SA were blocked (HJ24-bio tip/blocked SA). The last rupture forces of these control experiments were measured and compared. The results are shown in Figure 4 in red, and the corresponding force histograms are presented in Figure S1 in the Supporting Information.

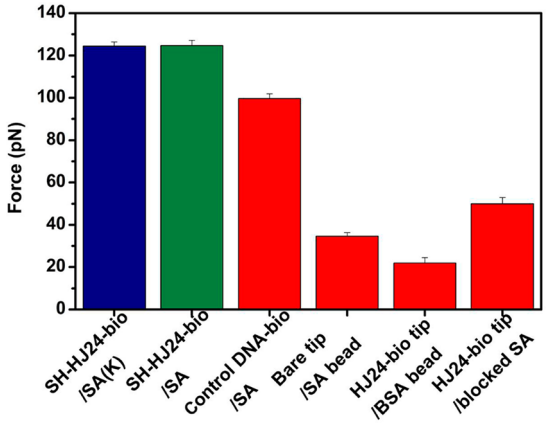

Figure 4. Rupture forces associated with biotin−SA interaction (SH-HJ24-bio) in the presence (blue) and absence (green) of K^+ and four control experiments (red). Each data in the graph refers to the most probable rupture force value.

Compared with the dual-labeled random sequence DNA/SA system (control DNA-bio/SA), a further significant decrease of the binding force is observed in the control experiments with systems lacking either the ligand (bare tip/SA bead) or the receptor (HJ24-bio tip/BSA bead). Especially, in the HJ24-bio tip/blocked SA control experiment, a significant decrease of about 50% of the unbinding probability is observed, although the corresponding force is higher than other control tests due to the persistence of a residual binding activity of the HJ24-bio to the SA after blocking. Such a residual activity likely arises from the forced interaction between two molecules nearby[48] and possibly due to the interaction of HJ24-bio with the blocked SA through nonspecific and noncovalent interactions including charge interaction, hydrogen bonding, etc. Overall, these control experiments confirm that the last rupture forces measured in the systems employing the biotin-functionalized SMFS tip and the SA-functionalized bead surface are most likely caused by the specific unbinding events between the biotin end of the dual-labeled G-quadruplex and the SA protein.

The bio−SA rupture force histograms for dual-labeled HJ24 G-quadruplex DNA and dual-labeled random sequence DNA in the presence and absence of K^+ ion are presented in Figure 4. The force between the biotin at the end of dual-labeled HJ24 aptamer and SA stays at 124.5 pN regardless of whether or not K^+ is present. This value is smaller than those reported in the literature, e.g., 160 pN by the Gaub group.[49] The exact value is expected to depend on the molecules onto which the biotin is attached and the differences in the experiment conditions such as pH and ionic strength of solutions. This also explains the difference in bio−SA rupture force obtained for dual-labeled HJ24 G-quadruplex DNA and dual-labeled random sequence DNA.

Melting Force of HJ24 Secondary Structure and Influence of K^+. Since we have attributed the last rupture force on the force curve to bio−SA unbinding, the K^+ ion influence on conformational stability of the G-quadruplexes may be investigated further by measuring the melting force associated with the second last of the force transitions upon stretching the molecule. Since the control DNA (see Table 1) contains neither the consensus structural sequence of HJ24 G-quadruplex aptamer (SH-HJ24-bio) nor other type of intricate secondary structure, it was therefore employed as a reference for discriminating nonspecific adhesion force from the G-quadruplex melting force. Histograms of melting forces for control DNA in the presence of K^+ and HJ24 in the presence and absence of K^+ are shown in Figure 5. It can be seen that HJ24 in the presence of K^+ shows only a single peak of melting force at 49.7 pN, while HJ24 in the absence of the K^+ exhibits double peaks located at 16.9 and 39.0 pN, respectively. For the control DNA, however, even in the presence of K^+, there exists only a single force peak at 27.5 pN.

In order to analyze the melting probability, we evaluated ratios between successful events corresponding to HJ24 melting processes over the total recorded events and biotin/SA complex rupture events, respectively. The results are given in Figure 6. It can be seen that the melting probability with respect to total successful event (i.e., bio−SA rupture events) is 25.8% for HJ24 with K^+ in contrast to 4.8% for HJ24 without K^+ and 3.5% for control DNA. For HJ24 in the absence of K^+, two melting peaks appear in the histogram. In this case, the successful rate associated with each peak is also estimated by multiplying the peak area and the probability (4.8%). In addition, the melting force of HJ24 in the presence of K^+ is 49.7 pN, which is significantly higher than that observed in the absence of K^+ (38.6 pN) and control DNA (27.5 pN). An explanation for this is that potassium ions are involved in G-quadruplex formation[50] that is necessary for strong binding of the aptamer with the proteins. The observed stronger adhesion between the probe and the substrate in the presence of 60 mM K^+ is further confirmed by our CD measurement.[51] Notably, for HJ24 in the absence of K^+, peak I at 16.9 pN and peak II at 39.0 pN, Figure 5b, are close to that of control DNA at 27.5 pN and HJ24 in the presence of K^+ at 49.7 pN, respectively, although both are shifted toward lower values. The peak area ratio for peak I and II is 1:3. This suggests that the HJ24 in pure water

dx.doi.org/10.1021/jp303518b | J. Phys. Chem. B 2012, 116, 11397−11404

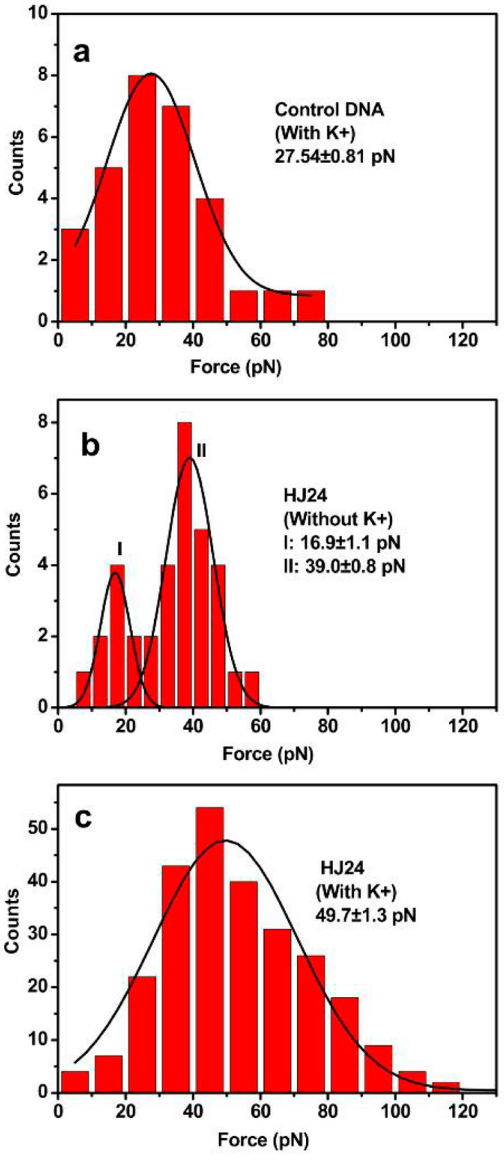

Figure 5. Force histograms of control DNA (a) and HJ24 in the absence (b) and presence (c) of K^+. Gaussian fittings are performed for peak forces. The data outlined refer to the most probable rupture forces.

may exhibit alternating folding and unfolding patterns as a result of dynamic equilibrium.[52]

Binding Affinity of HJ24 and Shp2. As shown in Figure 1b, the specific interaction between the HJ24 G-quadruplex aptamer and target protein Shp2 phosphatase can be investigated by employing the HJ24 G-quadruplex aptamer as the probe. For this purpose, HJ24 G-quadruplex is labeled only with T_{20}-SH at the 3′ end. Typical force curves and force histograms of HJ24/Shp2 complex rupture in the presence and absence of K^+ are shown in Figure 7. The response of the HJ24/Shp2 complex to the retraction of the AFM tip depends on the stability of the complex with respect to that of the HJ24 in the complex. Assuming that the HJ24 is sufficiently stable before the rupture of the HJ24/Shp2 complex upon stretching, the measured rupture force should contain only the unbinding of the HJ24/Shp2 complex. In other words, only single rupture force should appear on the force curves, which can indeed be discerned by the force curves for the HJ24/Shp2 complex; see

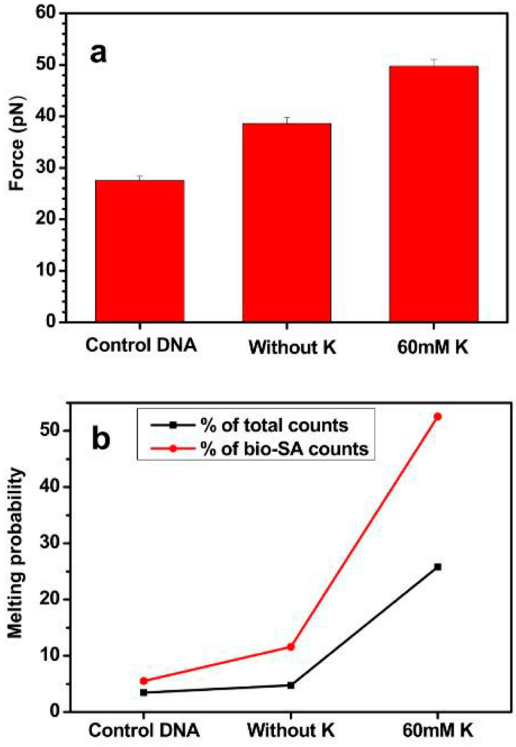

Figure 6. (a) Melting force in the absence and presence of K^+ as well as of control DNA. (b) Binding percentages for HJ24 in both solutions and with control DNA. Each data point on the histograms refers to the most probable rupture force.

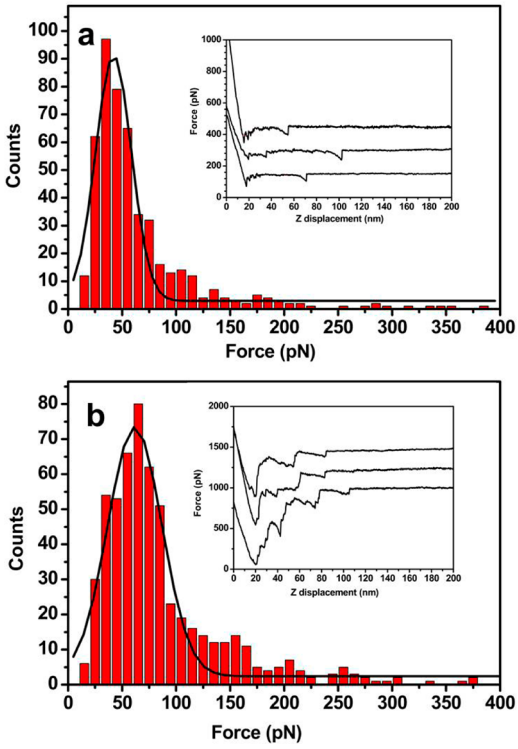

Figure 7. Force histograms of the HJ24 G-quadruplex DNA aptamer interaction with the oncogenic protein Shp2 in the solution without K^+ ion (a) and with 60 mM K^+ (b). Insets are corresponding typical force curves recorded upon tip retracting.

dx.doi.org/10.1021/jp303518b | J. Phys. Chem. B 2012, 116, 11397−11404

inset in Figure 7a. (We mention that the noisy feature on the force curve of Figure 7b arises from the ill-defined conformation of the beads employed. Use of flat Si substrate suppresses the noisy feature so that a clear single rupture force on the force curve is also obtained in the presence of K^+, Figure S3, Supporting Information.) However, single peak force curves do not exclude the possibility of induced dissociation of the complex by the weakening of the H-bonding of the G-quadruplex aptamer upon retraction of the AFM tip, which may proceed almost simultaneously within the time scale of the measurements. In this case, only part of the rupture force is contributed by the unbinding of the complex. The rupture forces measured in the presence and absence of K^+ are depicted by the blue and green pillars, respectively, in Figure 8. The

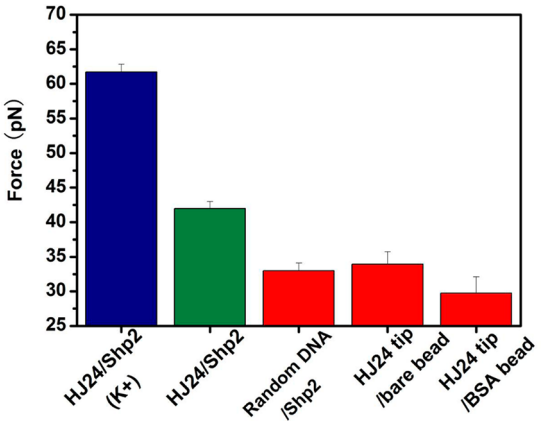

Figure 8. Rupture forces of G-quartet aptamer HJ24 with protein Shp2 in different environments and several control experiments. Each data point on the histograms refers to the most probable rupture force obtained by Gaussian fitting of the corresponding force histogram.

corresponding force distribution is presented in Figure S2 (Supporting Information). The HJ24/Shp2 unbinding force in the absence of K^+, 42.0 pN, is about 50% smaller than that in the presence of K^+, 61.7 pN. The great reduction in force in the absence of K^+ suggests that the stability of the G-quadruplex secondary structure is important for a stable HJ24/Shp2 binding.

In order to understand the role of the secondary structure of G-quadruplex on the HJ24/Shp2 interaction, three control experiments were carried out using (1) a random sequence DNA modified SMFS tip, (2) a bare SMFS tip, and (3) a BSA modified bead substrate lacking the Shp2 protein. The results of these control experiments are summarized in Figure 8. The force value from random DNA/Shp2 is dramatically reduced compared with those of HJ24/Shp2 with and without K+, implying that molecular level specific adhesion force does not exist between the random sequence DNA motif and the Shp2 protein because of lack of a specific secondary structure. Even in the absence of K^+, the binding force of HJ24-Shp2, 42.0 pN, is remarkably higher than that of the random DNA-Shp2 control. This indicates that either the remaining G-quadruplex secondary structure of the HJ24 aptamer, supra vide, or an induced folding conformation of the HJ24 aptamer upon contact with the Shp2 protein are in favor of interaction with the target Shp2 protein to a certain degree even in the pure water. This is consistent with the binding study with flow cytometry assay (Figure S4, Supporting Information).

Finally, the force measured between the HJ24 G-quadruplex aptamer and the Shp2 protein is within the range of usual antigen−antibody interaction force values[37] (several tens to more than one hundred piconewtons). Control experiments have revealed that the measured rupture force value is larger than the melting force of random DNA, which indicates the presence of a specific binding mode in the complex. This is of biological significance. Furthermore, the influence of K^+ on the rupture force of HJ24 and thus the complex clearly indicates the importance of G-quadruplex conformation on the binding affinity.

CONCLUSIONS

We have demonstrated an improved dual-labeling approach for surface attachment of an integral unimolecular G-quadruplex aptamer, which can be used to functionalize the AFM probes for single molecule force measurement to investigate the structural stability of G-quadruplex systems. The stability of the secondary structure of unimolecular HJ24 G-quadruplex aptamer in the presence of K^+ has been successfully investigated by single molecule force spectroscopy, and the measured melting force is 49.7 pN. It has also been found that the HJ24 aptamer in pure water exhibits a dynamic equilibrium between two conformations of unfolding and folding states, the melting force of the latter being close to that in the presence of K^+. The dual-labeling method may also be used for investigating other unimolecular intramolecular G-quadruplexes. By using single-end-labeled G-quadruplex SMFS probes, we have also studied molecular interaction of HJ24 aptamer/Shp2 target protein. The HJ24/Shp2 unbinding force in the absence of K^+, 42.0 pN, is about 50% smaller than that in the presence of K^+, 61.7 pN. The great reduction in force in the absence of K^+ suggests that the stability of G-quadruplex secondary structure is important for a stable HJ24/Shp2 binding. The methodology developed and demonstrated in this work is applicable for studying the stability of secondary structures of other unimolecular G-quadruplex aptamers and their interactions with target proteins.

ASSOCIATED CONTENT

Supporting Information

The force histograms of biotin−SA interaction and control experiments for HJ24 and Shp2 interaction, typical force curves on Si substrate, and flow cytometry assay. This material is available free of charge via the Internet at http://pubs.acs.org.

AUTHOR INFORMATION

Corresponding Author

*Phone/Fax: +86 05922186862. E-mail: cyyang@xmu.edu.cn (C.J.Y.); bwmao@xmu.edu.cn (B.-W.M.).

Notes

The authors declare no competing financial interest.

ACKNOWLEDGMENTS

The authors are grateful to Prof. Xiao-Hong Fang and her group, Institute of chemistry, Chinese academy of China, for providing experimental support and sharing of knowledge. This work was supported by National Natural Science Foundation of China (No. 21021002), National Basic Research Program of China (2010CB732402), and the Natural Science Foundation of Fujian Province for Distinguished Young Scholars (2010 J06004).

REFERENCES

(1) Phan, A. T. *FEBS J.* **2010**, *277*, 1107−1117.
(2) Neidle, S.; Balasubramanian, S. *Quadruplex Nucleic Acids*; RSC Biomolecular Sciences: Cambridge, U.K., 2006.
(3) Eddy, J.; Maizels, N. *Nucleic Acids Res.* **2006**, *34*, 3887−3896.
(4) Hardin, C. C.; Perry, A. G.; White, K. *Biopolymers* **2000**, *56*, 147−194.
(5) Sen, D.; Gilbert, W. *Nature* **1988**, *334*, 364−366.
(6) Sarkies, P.; Reams, C.; Simpson, L. J.; Sale, J. E. *Mol. Cell* **2010**, *40*, 703−713.
(7) Bejugam, M.; Sewitz, S.; Shirude, P. S.; Rodriguez, R.; Shahid, R.; Balasubramanian, S. *J. Am. Chem. Soc.* **2007**, *129*, 12926−12927.
(8) Patel, D. J.; Phan, A. T.; Kuryavyi, V. *Nucleic Acids Res.* **2007**, *35*, 7429−7455.
(9) Sannohe, Y.; Endo, M.; Katsuda, Y.; Hidaka, K.; Sugiyama, H. *J. Am. Chem. Soc.* **2010**, *132*, 16311−16313.
(10) Miyoshi, D.; Sugimoto, N. G-Quartet, G-Quadruplex and G-Wire Regulated by Chemical Stimuli. In *DNA Nanotechnology: Methods and Protocols*; Zuccheri, G., Samorì, B., Eds.; Humana Press: New York, 2008; Vol. *749*, pp 93−104.
(11) Alberti, P.; Bourdoncle, A.; Sacca, B.; Lacroix, L.; Mergny, J.-L. *Org. Biomol. Chem.* **2006**, *4*, 3383−3391.
(12) Morita, Y.; Yoshida, W.; Savory, N.; Han, S. W.; Tera, M.; Nagasawa, K.; Nakamura, C.; Sode, K.; Ikebukuro, K. *Biosens. Bioelectron.* **2011**, *26*, 4837−4841.
(13) Chen, Q.; Tang, W.; Wang, D.; Wu, X.; Li, N.; Liu, F. *Biosens. Bioelectron.* **2010**, *26*, 575−579.
(14) Renaud de la Faverie, A.; Hamon, F.; Di Primo, C.; Largy, E.; Dausse, E.; Delaurière, L.; Landras-Guetta, C.; Toulmé, J.-J.; Teulade-Fichou, M.-P.; Mergny, J.-L. *Biochimie* **2011**, *93*, 1357−1367.
(15) Nomura, Y.; Sugiyama, S.; Sakamoto, T.; Miyakawa, S.; Adachi, H.; Takano, K.; Murakami, S.; Inoue, T.; Mori, Y.; Nakamura, Y.; Matsumura, H. *Nucleic Acids Res.* **2010**, *38*, 7822−7829.
(16) Wang, Z.; Wilkop, T.; Xu, D.; Dong, Y.; Ma, G.; Cheng, Q. *Anal. Bioanal. Chem.* **2007**, *389*, 819−825.
(17) Shirude, P. S.; Balasubramanian, S. *Biochimie* **2008**, *90*, 1197−1206.
(18) Diculescu, V. C.; Chiorcea-Paquim, A. M.; Eritja, R.; Oliveira-Brett, A. M. *J. Electroanal. Chem.* **2011**, *656*, 159−166.
(19) Tinoco, I.; Gonzalez, R. L. *Genes Dev.* **2011**, *25*, 1205−1231.
(20) Deniz, A. A.; Mukhopadhyay, S.; Lemke, E. A. *J. R. Soc., Interface* **2008**, *5*, 15−45.
(21) Okumus, B.; Ha, T. Real-Time Observation of G-Quadruplex Dynamics Using Single-Molecule FRET Microscopy. In *G-Quadruplex DNA:Methods and Protocols*; Baumann., P., Ed.; Humana Press: New York, 2010; Vol. *608*, pp 81−96.
(22) Walter, N. G.; Huang, C.-Y.; Manzo, A. J.; Sobhy, M. A. *Nat. Methods* **2008**, *5*, 475−489.
(23) Hinterdorfer, P.; Dufrene, Y. F. *Nat. Methods* **2006**, *3*, 347−355.
(24) Liu, K.; Song, Y.; Feng, W.; Liu, N.; Zhang, W.; Zhang, X. *J. Am. Chem. Soc.* **2011**, *133*, 3226−3229.
(25) Yuan, C.; Chen, A.; Kolb, P.; Moy, V. T. *Biochemistry* **2000**, *39*, 10219−10223.
(26) Roy, D.; Kwon, S. H.; Kwak, J.-W.; Park, J. W. *Anal. Chem.* **2010**, *82*, 5189−5194.
(27) Alsteens, D.; Dupres, V.; Andre, G.; Dufrêne, Y. F. *Nanomedicine* **2011**, *6*, 395−403.
(28) Greene, D. N.; Garcia, T.; Sutton, R. B.; Gernert, K. M.; Benian, G. M.; Oberhauser, A. F. *Biophys. J.* **2008**, *95*, 1360−1370.
(29) Liu, N.; Peng, B.; Lin, Y.; Su, Z.; Niu, Z.; Wang, Q.; Zhang, W.; Li, H.; Shen, J. *J. Am. Chem. Soc.* **2010**, *132*, 11036−11038.
(30) Ling, L.; Butt, H.-J.; Berger, R. *J. Am. Chem. Soc.* **2004**, *126*, 13992−13997.
(31) Sattin, B. D.; Pelling, A. E.; Goh, M. C. *Nucleic Acids Res.* **2004**, *32*, 4876−4883.
(32) Soldatenkov, V. A.; Vetcher, A. A.; Duka, T.; Ladame, S. *ACS Chem. Biol.* **2008**, *3*, 214−219.
(33) Basnar, B.; Elnathan, R.; Willner, I. *Anal. Chem.* **2006**, *78*, 3638−3642.
(34) Jiang, Y.; Zhu, C.; Ling, L.; Wan, L.; Fang, X.; Bai, C. *Anal. Chem.* **2003**, *75*, 2112−2116.
(35) Björnham, O.; Schedin, S. *Eur. Biophys. J.* **2009**, *38*, 911−922.
(36) Nguyen, T.-H.; Steinbock, L. J.; Butt, H.-J. r.; Helm, M.; Berger, R. d. *J. Am. Chem. Soc.* **2011**, *133*, 2025−2027.
(37) Lee, C.-K.; Wang, Y.-M.; Huang, L.-S.; Lin, S. *Micron* **2007**, *38*, 446−461.
(38) Hu, J.; Wu, J.; Li, C.; Zhu, L.; Zhang, W. Y.; Kong, G.; Lu, Z.; Yang, C. J. *ChemBioChem* **2011**, *12*, 424−430.
(39) Tinland, B.; Pluen, A.; Sturm, J.; Weill, G. *Macromolecules* **1997**, *30*, 5763−5765.
(40) Parkinson, G. N.; Lee, M. P. H.; Neidle, S. *Nature* **2002**, *417*, 876−880.
(41) Clavilier, J.; Armand, D.; Sun, S. G.; Petit, M. *J. Electroanal. Chem. Interfacial Electrochem.* **1986**, *205*, 267−277.
(42) Wang, W.; Liu, H.; Liu, D.; Xu, Y.; Yang; Zhou, D. *Langmuir* **2007**, *23*, 11956−11959.
(43) Zhou, C. Q.; Tan, Z. K.; Wang, C.; Wei, Z. Q.; Wang, Z. G.; Bai, C. L.; Qin, J. F.; Cao, E. H. *J. Biomol. Struct. Dyn.* **2001**, *18*, 807−812.
(44) Rounsevell, R.; Forman, J. R.; Clarke, J. *Methods* **2004**, *34*, 100−111.
(45) Bizzarri, A. R.; Cannistraro, S. *Chem. Soc. Rev.* **2010**, *39*, 734−749.
(46) Grandbois, M. *Science* **1999**, *283*, 1727−1730.
(47) Lynch, S.; Baker, H.; Byker, S. G.; Zhou, D.; Sinniah, K. *Chem.—Eur. J.* **2009**, *15*, 8113−8116.
(48) Bizzarri, A. R.; Cannistraro, S. *J. Phys. Chem. B* **2009**, *113*, 16449−16464.
(49) Florin, E.; Moy, V.; Gaub, H. *Science* **1994**, *264*, 415−417.
(50) Morin, G. B. *Cell* **1989**, *59*, 521−529.
(51) Hu, J.; Wu, J.; Li, C.; Zhu, L.; Zhang, W. Y.; Kong, G. P.; Lu, Z. X.; Yang, C. J. *ChemBioChem* **2011**, *12*, 424−430.
(52) Taylor, A.; Taylor, J.; Watson, G. W.; Boyd, R. J. *J. Phys. Chem. B* **2010**, *114*, 9833−9839.